

Wearable Antennas for Body-Centric Communications: Design and Characterization Aspects

**Abdullah G. Al-Sehemi^{1,2}, Ahmed A. Al-Ghamdi³, Nikolay T. Dishovsky⁴,
Nikolay T. Atanasov⁵, and Gabriela L. Atanasova⁵**

¹ Research Center for Advanced Materials Science (RCAMS)
King Khalid University, Abha, 61413, Saudi Arabia
agsehemi@kku.edu.sa

² Department of Chemistry
King Khalid University, Abha, 61413, Saudi Arabia
agsehemi@kku.edu.sa

³ Department of Physics
King Abdulaziz University, Jeddah, Saudi Arabia
aghamdi90@hotmail.com

⁴ Department of Polymer Engineering
University of Chemical Technology and Metallurgy, Sofia, 1756, Bulgaria
dishov@uctm.edu

⁵ Department of Communication and Computer Engineering
South-West University 'Neofit Rilski', Blagoevgrad, 2400, Bulgaria
natanasov@windowslive.com, gatanasova@windowslive.com

Abstract — Wearable antennas exhibit numerous challenges in terms of design and optimization due to the specific environment in which they operate. Therefore, the design of such antennas is a non-trivial task, as multiple constraints have to be satisfied. We present an algorithm for design-and-optimization of flexible wearable antennas with high radiation efficiency and low specific absorption rate, that takes into account the dielectric loading of the human body. It provides a list of feasible antenna designs, not just a single solution, and identifies the optimal wearable antenna design. Numerical examples on the design and optimization of a wearable antenna (based on a dipole structure with a reflector) to demonstrate the validity and efficiency of the proposed algorithm are given. The optimal antenna design shows robust on-body performance and provides a suitable balance between small antenna size (antenna surface is 2214 mm²), high radiation efficiency (57.73%), and low value of the maximum 10 g average SAR (0.112 W/kg) on a homogeneous semisolid phantom. Finally, the optimal antenna design is fabricated. The antenna performance is studied under different conditions: on a homogeneous semisolid phantom, on a liquid phantom, on a three-layer semisolid phantom, on a human arm and

in the free space. A good agreement between simulated and measured antenna performance is observed.

Index Terms — Antenna characterization, antenna design, optimization, radiation efficiency, SAR, wearable antenna.

I. INTRODUCTION

Body-centric wireless communications (BCWCs) are held to have the potential to improve the quality of life and could offer significant benefits in commercial, military and medical applications, personal entertainment, and so on and so forth [1-6]. They will also play an important role in the upcoming era of the Internet of Things. Such systems provide short range low-power, and highly reliable wireless connectivity between devices worn on (or implanted in) the human body, or between two devices (body-to-body or body-hub) in close proximity. Consequently, three wireless communication channels (in-, on-, and off-body) exist.

The wearable antenna and radio wave propagation constitute the basic elements of the on- and off-body wireless channel. They determine reliability of the wireless link and have a great impact on the quality-of-

service offered by the whole system [7]. Therefore, the antenna design is a topic of great importance.

The wearable antennas exhibit numerous challenges in terms of design and optimization. For example, to achieve a good performance in a BCWCs system the wearable antenna should be insensitive to the effects of the human body in order to minimize detuning of the resonant frequency and degradation of the radiation efficiency. At the same time, the impact of the wearable antenna on human tissues also needs to be addressed, such as the maximum allowed specific absorption rate (SAR) [8]. The wearable antennas also should be compact, lightweight, and flexible, possibly allowing for integration with clothes and garment accessories [9]. Another limitation in the design of wearable antennas in which substrates are from textiles or polymer materials is finding of electromagnetic properties of the materials. In addition, these antennas have to show good radiation characteristics and high radiation efficiency [4]. Consequently, in wearable antenna design and optimization problems, several goals (impedance matching, bandwidth, compact size, high radiation efficiency, and low SAR) must be satisfied simultaneously in order to obtain an optimal solution.

An algorithm for flexible and wearable antenna design has been proposed in [10]. The proposed design procedure is mainly focused on the selection of the materials and on the analysis of the antenna structure in the free space, without to investigate the effect of the human body proximity on the antenna performance. In [11] the problem of optimization design of a microwave wearable antenna jointly with the model of human body that is located in the proximity of the antenna has been investigated. The presented optimization procedure uses full wave simulator based on finite difference time domain method (FDTD) to improve antenna design with respect to its impedance matching for several values of the antenna-to-body distance. In both [10] and [11], the antenna efficiency is not reported.

Recently, a number of algorithms like, ant colony optimization (ACO) [12], genetic algorithm (GA) [13, 14], and particle swarm optimization (PSO) [13] have been introduced for antennas aimed at either improving the current design or at speeding up the design process [15]. All of these algorithms are random search algorithms that are guided by biological principles. They all maintain a collection of possible solutions and use biologically based rules to search the objective function space for the best solution [13]. However, as the number of variables increase, the search space size grows exponentially, making it harder for these algorithms to find a suitable solution [16].

Multi-objective optimization has been presented for problems with more than one objective and its application to antennas for ground penetrating radar, satellite broadcast communications, and RFID tags has

been reported in [17].

In this work, we firstly propose an improved algorithm for wearable antenna numerical design-and-optimization. The algorithm is based on the ideas in [13, 17] and has the advantage to provide a list of feasible antenna designs and to find the optimal solution that meets specifications. Next it is demonstrated using a planar dipole antenna. The presented algorithm can be quickly adopted in practice and applied to any wearable antenna structure.

The novelty in our work lies in the fact that we present a fast design of compact and flexible wearable antennas with high radiation efficiency and low SAR, that takes into account the dielectric loading of the human body.

II. NUMERICAL DESIGN-AND-OPTIMIZATION ALGORITHM

In this section in Fig. 1, we describe the proposed algorithm for wearable antenna numerical design-and-optimization. The principal difficulty in the design of a compact flexible wearable antenna is that both the human body and size miniaturization may affect antenna performance (such as resonant frequency, bandwidth and/or radiation efficiency).

Taking into consideration the above factors the first step in wearable antenna design is the selection of design goals and stopping criteria. We propose the following design goals: (1) minimization of the overall antenna size, (2) minimization of the reflection coefficient magnitude ($|S_{11}|$) at the desired resonant frequency (f_r), (3) maximization of the antenna radiation efficiency (RE), and (4) minimization of the specific absorption rate (SAR). The stopping criteria associated with these design goals can be expressed as: (1) First stopping criteria: $|S_{11}| \leq -15$ dB at f_r , $|S_{11}| \leq -10$ dB within the frequency band of interest, and $f_L \leq f_r \leq f_U$, (2) Second stopping criteria: $RE \geq 50$ % and $SAR \leq 0.5$ W/kg.

The next steps in the wearable antenna design are the selection of antenna topology and a suitable selection of materials, both for the conductive and nonconductive parts of the antenna [18]. A detailed review of available topologies for wearable antennas can be found in [3, 18-21] and a survey of the different types of materials for wearable antennas can be found in [3, 18, 21]. As mentioned above, the wearable antennas should be designed on flexible materials. Flexible materials like fabrics, polymers, and papers have been widely used in the existing wearable antennas. Consequently, the next important step when designing antennas on fabrics or polymer materials is a characterization of the electromagnetic (EM) properties of the materials like complex relative permittivity and/or permeability, loss tangent, and electric conductivity.

Once the antenna topology and materials for the conductive and nonconductive parts of the antenna

are selected and their electromagnetic properties are characterized, the next step is to provide an initial design of the wearable antenna. The initial antenna design has to originate from human experience, knowledge, innovation [22], and from a set of dimensional formulas. It includes techniques to design antenna elements and for generating a set of preliminary input design data for numerical full-wave EM analysis. Once the initial design of the antenna is known, the geometrical parameters for the optimization process have to be carefully selected and defined. In the next step third stopping criteria associated with geometrical parameters of the antenna (lower bound \leq antenna geometrical parameters \leq upper bound) also have to be provided.

Moreover, the design of one antenna for body-centric communications has to be carried out taking into account the human body effects [23]. Consequently, experimental and numerical phantoms of the human body have to be developed and their EM properties have to be extracting. A detailed review of various types of phantoms is presented in [9, 24]. The phantoms shapes, size, and electrical properties of the tissue-equivalent liquids are also provided in EN 62209-2-2010 [25], IEEE Std. 1528-2003 [26], and FCC 865664 D01 [27].

The next step in the numerical design-and-optimization algorithm is to build a numerical model of the antenna and phantom taking into account the electromagnetic properties of the materials. The last step before launching the EM simulations is the simulation parameters setup (boundary conditions, excitation, meshing). This is presented in Fig. 1 through the block labelled “Preprocessor”. Various numerical methods are available in the literature, each with specific advantages and drawbacks, making them suitable for analysis, modeling, simulation, design and visualization of wearable antennas. These methods include Finite-Difference Time-Domain, Integral Equations/Method of Moments (MoM), Finite Element Method (FEM) [22].

The FDTD is probably the most popular technique for the analysis of wearable antennas. Reasons for its popularity include its versatility, low computational complexity, ability to accurately determine near- and far-field antenna characteristics over a wide frequency bandwidth from a single time domain simulation in the presence of complex materials (anisotropic, inhomogeneous and frequency dispersive). One drawback of the FDTD is the approximation of curved surfaces, due to the “staircasing” caused by the use of cubic cells [9].

MoM can be applied to structures made either of good conductors such as a wire antenna or being well described by an impedance boundary condition. This method is inefficient for the analysis of wearable antennas with complex materials (anisotropic and inhomogeneous) and its numerical cost grows very fast with increase of the upper corner frequency.

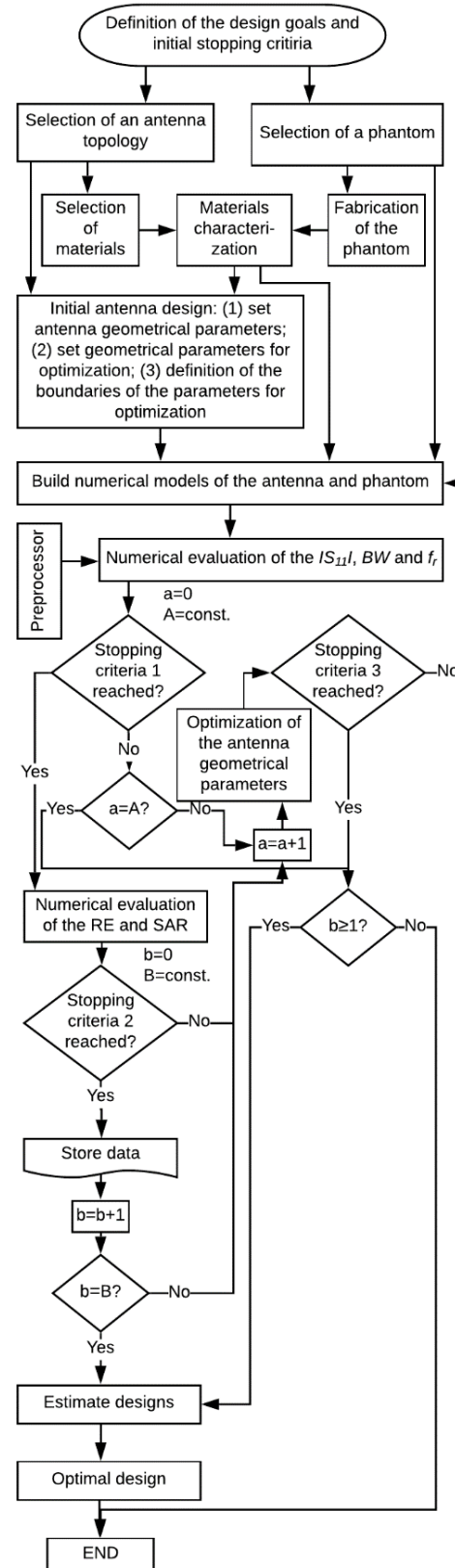


Fig. 1. A flowchart of the proposed design-and-optimization algorithm.

FEM is a frequency domain technique for the analysis and design of highly complicated antennas. The advantages of FEM are the flexibility in terms of modeling any complex geometries, irregular shapes, and inhomogeneous or dispersive materials. However, for geometrically and electrically large structures (such as the human body), the mesh can become very complex with many tetrahedral mesh cells. This in turn leads to huge matrices to solve which can require very large amounts of computer memory.

The optimization procedure starts from a cycle that selects new antenna design that satisfies the first stopping criteria ($|S_{11}| \leq -15$ dB at f_r , $|S_{11}| \leq -10$ dB within the frequency band of interest, and $f_L \leq f_r \leq f_U$), evaluates it, and subsequently updated numerical antenna model continues until a threshold is met or when the number of iterations exceeds a predefined maximum number of iterations ($A = \text{max number of iterations}$). The optimal antenna design obtained in the previous iteration of the optimization procedure is utilized as a starting point for the next optimization cycle. The cycle selects an antenna design that satisfies the second stopping criteria and stops when a threshold (finding the $B = \text{defined number of designs that satisfy second stopping criteria or after a defined maximum number of iterations}$) is met.

III. ILLUSTRATION EXAMPLES

In this section, we demonstrate the proposed algorithm for wearable antenna numerical design-and-optimization using a planar dipole structure, providing a compact flexible antenna with high radiation efficiency and low SAR for on-/off-body communications in the 2.4-2.48 GHz industrial, scientific, and medical (ISM) band.

The design goals for our first example are: (1) minimization of the overall antenna size, (2) minimization of the reflection coefficient magnitude at $f_r = 2.44$ GHz, (3) maximization of the antenna radiation efficiency, and (4) minimization of the specific absorption rate.

The proposed stopping criteria have been applied. In this example a dipole structure with a reflector has been selected and used as a candidate for evaluation of the proposed algorithm. The initial design of the antenna geometry is based on our earlier work [23] which demonstrated that the dipole antenna with a reflector is less affected by the presence of a human body model and consequently it is suitable for BCWCs.

Figure 2 (a) illustrates the geometry of dipole structure and microstrip line applied in the design of the wearable antenna. They are described by means of 10 geometrical parameters. Figure 2 (b) illustrates the overall geometry of the proposed wearable antenna. It is comprised of two components: (1) a planar dipole and a microstrip line which are placed on the first and second layer of a three-layer flexible dielectric material, and (2)

a metallic reflector which is placed on the third layer of the dielectric material. The overall geometry of the proposed wearable antenna is described by two geometrical parameters – width (W) and length (L). Stopping criteria 3 associated with geometrical parameters of the antenna is defined: $37.5 \text{ mm} \leq W \leq 44 \text{ mm}$ and $48 \text{ mm} \leq L \leq 56 \text{ mm}$.

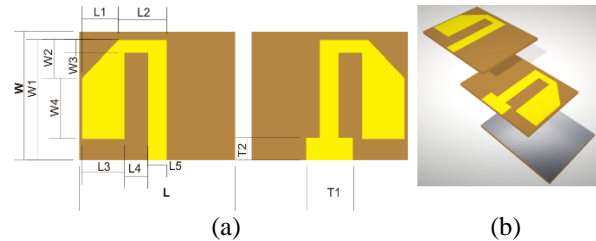


Fig. 2. The geometry of the: (a) dipole structure and (b) wearable antenna.

A brass foil with a thickness of 0.05 mm (for the radiating elements) and an aluminum foil with a thickness of 0.01 mm (for the reflector) are selected and used for the conductive parts of the antenna. For nonconductive parts of the antenna a composite based on natural rubber mixed with kaolin as a filler is synthesized and used. The rubber composite is selected as the antenna's substrate due to its notable features, such as high flexibility, ability to withstand mechanical strains and low dielectric loss. The electromagnetic parameters of the synthesized rubber composite were measured by the resonant perturbation method which is a well-known method for extracting electromagnetic properties of dielectrics, semiconductors, magnetic materials, and composite materials [28]. The real part of the relative permittivity is 2.481, imaginary part is 0.015, and the dielectric loss angle ($\tan\delta$) is 0.006 at 2.56 GHz.

Three different types of the human body phantoms are developed and fabricated. The first one is a homogeneous semisolid (gel) phantom with dimensions $100 \text{ mm} \times 47 \text{ mm} \times 117 \text{ mm}$ and measured EM parameters to emulate human muscle tissue (relative permittivity $\epsilon_r' = 40.81$ and conductivity $\sigma = 2.33 \text{ S/m}$ at 2.56 GHz). The EM properties of the phantom are in agreement with those of 2/3 muscle [29] (relative deviation within 15%). The second one is a liquid phantom. This phantom is widely used in SAR evaluation and can quite well represent tissues with high water content. The liquid phantom is a rectangular box with dimensions $300 \text{ mm} \times 150 \text{ mm} \times 360 \text{ mm}$ made of Plexiglas having 2 mm thickness (phantom shell), filled with deionized water. The EM parameters of the liquid numerical phantom at 2.45 GHz are $\epsilon_r' = 78.69$, $\sigma = 1.44 \text{ S/m}$ [26] for deionized water and $\epsilon_r' = 2.67$, $\tan\delta = 0.007$ for the phantom shell. The third one is a three-layer semisolid model, consisting of skin, fat and muscle tissue

layers. The EM parameters and thickness of the different tissue layers of three-layer phantom in numerical calculation at 2.45 GHz are presented in Table 1 and assumed to be in [29].

Table 1: Material properties and thickness of three-layer semisolid phantom in numerical calculation

	ϵ_r'	σ (S/m)	ρ (kg/m ³)	Thickness (mm)
Skin	38.006	1.464	1020	1.0
Fat	5.280	0.105	918	6.0
Muscle	53.574	1.81	1040	40.0

The numerical models of the antenna and homogeneous phantoms (semisolid and liquid) are simulated in XFDTD (xFDTD, Remcom Inc., State College, PA, USA) a software that utilizes the finite-difference time-domain method. Each simulation is accomplished under the following conditions: a non-uniform cubic-cell mesh (cell size of 0.5 mm and 5 mm) and a perfectly matched layer (7 layers) is used at the boundaries of the computational domain. The 12-field components approach is used to calculate SAR in the voxel.

To simplify antenna geometry generation, the numerical models of the dipole structure and microstrip line are first optimized on the homogeneous semisolid phantom and all 10 variables of the geometrical parameters are updated to meet the design specifications. The resulting design parameter values have been achieved in 152 iterations and are listed in Table 2. The antenna is directly placed onto the surface of the semisolid phantom, as in Fig. 3 (a).

Table 2: Parameter values of the dipole structure and microstrip line, which have been optimized by dint of the proposed algorithm for wearable antenna design

Parameter	Value (mm)	Parameter	Value (mm)
L1	12.0	W2	12.0
L2	15.5	W3	4.0
L3	13.5	W4	19.0
L4	7.5	T1	15.0
L5	6.0	T2	7.0

Next numerical optimization of the wearable antenna is performed in two steps. In the first step a number of solutions (optimized antenna structures) that satisfy the first stopping criteria are found. These are obtained through update of the parameters W and L of the numerical antenna model in an iterative way until a threshold (the number of solutions exceeds 25) is met or when the number of iterations exceeds 50. At each

iteration is generated a new numerical model of the antenna directly placed onto the surface of the numerical semisolid phantom and a simulation in XFDTD is launched. Figure 4 shows the obtained number of 22 solutions. Each point denotes a feasible design solution with three coordinates. Each design solution is denoted by the geometrical parameters W (mm) x L (mm) (width (mm) x length (mm) of the antenna). From Fig. 4, it can be seen that the antenna size is reduced from 2,464 mm² to 1,968 mm² (miniaturization ratio of 20%). The designs are utilized as starting points for the next step of the algorithm.

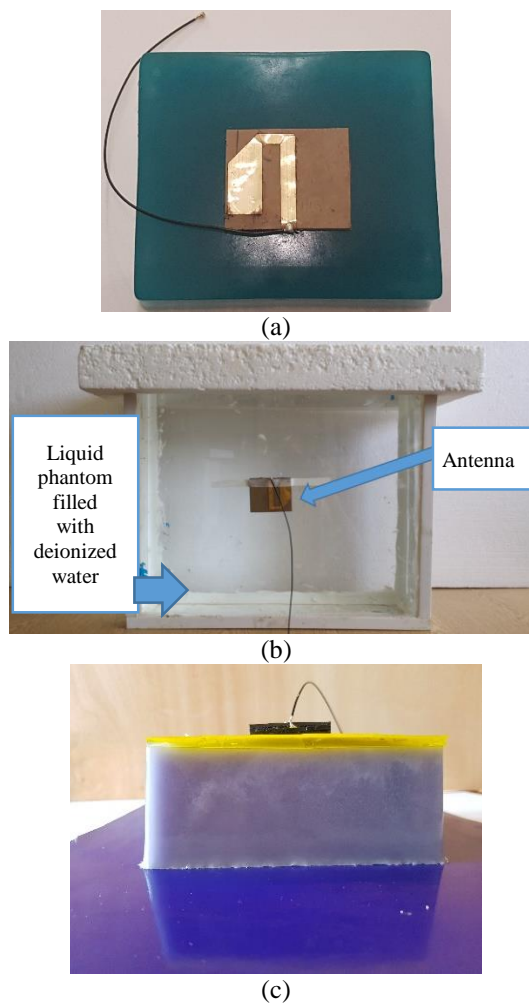


Fig. 3. Photographs of the fabricated human body phantoms with a prototype of the wearable antenna: (a) homogeneous semisolid, (b) liquid, and (c) three-layer semisolid.

In the next step radiation efficiency and SAR of the optimized antenna structures are estimated. The cycle selects antenna designs that satisfy second stopping criteria. Figure 5 shows the obtained number of 22

solutions (optimized antenna structures) after 40 iterations.

Design 44 x 56 provides the highest radiation efficiency (60.23%) and lowest maximum 10 g average SAR (0.103 W/kg) among all designs but no benefits in antenna size reduction (antenna surface is 2,464 mm²) and bandwidth. Design 41 x 48 shows a significant size reduction (about 20%) and bandwidth enhancement compared with other designs, but it presents also lowest radiation efficiency (52.54%). Consequently, there is a large trade-off between the achieved size reduction and the radiation efficiency. Design 41x54 is an optimal antenna design that provides a suitable compromise between the small antenna size (antenna surface is 2,214 mm²), high radiation efficiency (57.73%) and low value of the maximum 10 g average SAR (0.112 W/kg) in the ISM band.

The next verification of the proposed algorithm involved the design and optimization of a wearable antenna directly placed on the surface of a liquid phantom.

The design goals are same as for the first example. Again, first a number of solutions (optimized antenna structures) that satisfies the first stopping criteria are found and utilized as starting points for the next step.

In the next step radiation efficiency and SAR of the optimized antenna structures are estimated. Figures 6 and 7 show the obtained number of 20 solutions. It can be observed that the antenna size is reduced from 2,464 mm² to 1,920 mm² (miniaturization ratio of 22%). Designs 41 x 50 - to - 41 x 56 have the same SAR values (0.094 W/kg) but they are different in terms of radiation efficiency and bandwidth. Similarly, as for the previous example, design 44 x 56 provides the highest radiation efficiency (59.31%) and lowest maximum 10 g average SAR (0.059 W/kg) among all designs but no benefits in antenna size reduction (antenna surface is 2,464 mm²) and bandwidth.

Design and optimization of the proposed wearable antenna on the homogeneous liquid phantom lead to negligible enhancement of the bandwidth and reduction of maximum 10 g average SAR values compared to the semisolid phantom. The reason to obtain these results can be explained by the location of the antenna to the phantoms. For the semisolid phantom, the antenna touches to the surface of the phantom, and this makes the higher SAR values. Compared to the semisolid phantom, the liquid phantom has a thin shell (2 mm), which does not allow the estimation of the SAR on the phantom surface.

The last verification of the proposed algorithm involved the design and optimization of a wearable antenna directly placed on the surface of a three-layer phantom. The design goals and steps are same as for the first and second example. Figures 8 and 9 show the obtained number of 22 solutions.

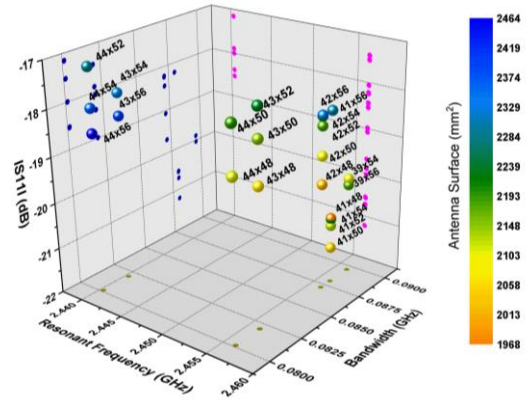


Fig. 4. A set of solutions satisfying constraints in first stopping criteria, obtained using the proposed algorithm. The wearable antenna is placed on a homogeneous semisolid phantom.

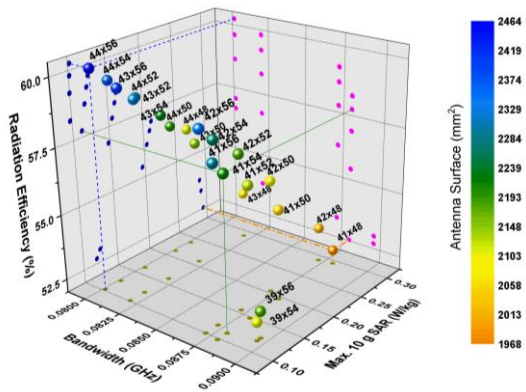


Fig. 5. A set of solutions satisfying constraints in second stopping criteria, obtained using the proposed algorithm. The wearable antenna is placed on a homogeneous semisolid phantom.

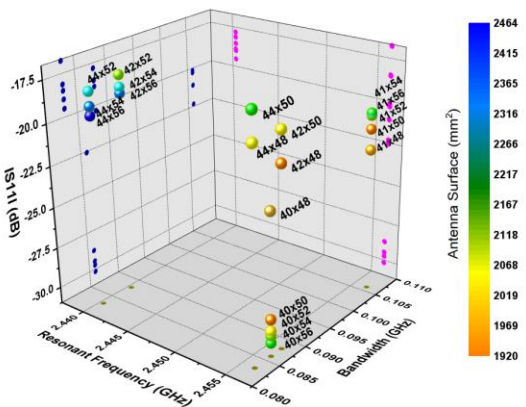


Fig. 6. A set of solutions satisfying constraints in first stopping criteria, obtained using the proposed algorithm. The wearable antenna is placed on a liquid phantom.

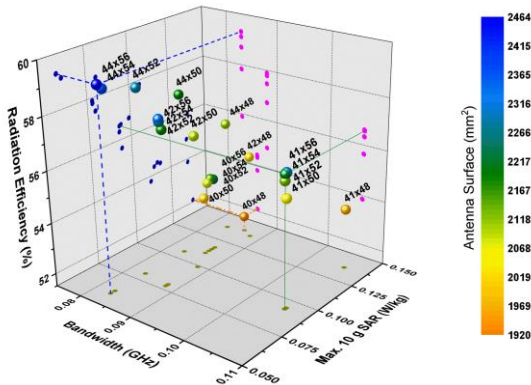


Fig. 7. A set of solutions satisfying constraints in second stopping criteria, obtained using the proposed algorithm. The wearable antenna is placed on a liquid phantom.

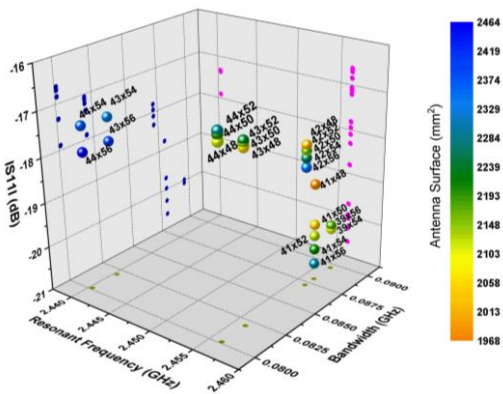


Fig. 8. A set of solutions satisfying constraints in first stopping criteria, obtained using the proposed algorithm. The wearable antenna is placed on a three-layer semisolid phantom.

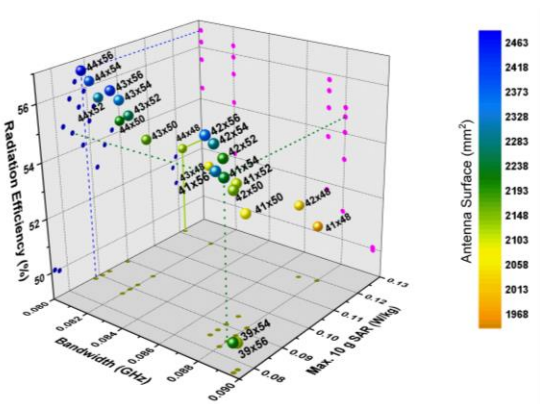


Fig. 9. A set of solutions satisfying constraints in second stopping criteria, obtained using the proposed algorithm. The wearable antenna is placed on a three-layer semisolid phantom.

Design and optimization of the proposed wearable antenna on the three-layer phantom lead to negligible reduction of the radiation efficiency (from 60.23% on homogeneous phantom to 56.20% on three-layer phantom for design 44 x 56) and reduction of maximum 10 g average SAR values compared to the homogeneous semisolid phantom.

IV. EXPERIMENTAL VALIDATION

In order to verify the proposed algorithm a prototype of the selected design 41 x 54 (width (mm) x length (mm) of the antenna) of the wearable antenna has been fabricated. The antenna performance in terms of reflection coefficient magnitude, bandwidth and radiation efficiency is analyzed under different conditions.

The measured and simulated $|S_{11}|$ curves of the optimized design are shown in Fig. 10. The experimental results are obtained when the antenna is mounted on the surface of the semisolid phantom and on the shell of the liquid phantom, as shown in Fig. 3. The results for antenna performance in the free-space and on human arm are also presented in Fig. 10 for comparison. It can be seen that, the measured $|S_{11}|$ curves agree well with the simulated curves. Moreover, the antenna exhibits a measured operating ($|S_{11}| \leq -10$ dB) bandwidth of 118 MHz on the semisolid phantom, 119 MHz on the liquid phantom, 119 MHz on human arm and 95 MHz in the free space. The simulated operating bandwidth of the proposed antenna on the semisolid phantom is 88 MHz, 106 MHz on the liquid phantom and 94 MHz in the free space. A good agreement between simulated and measured results is observed.

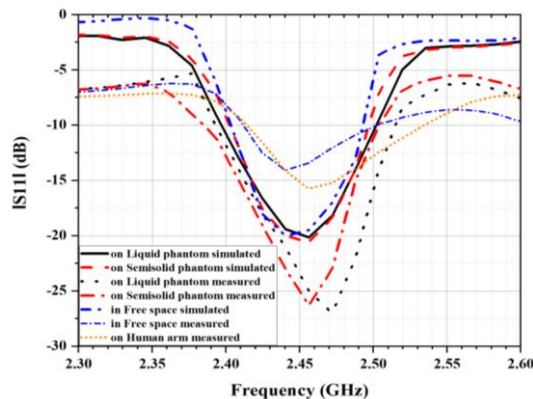


Fig. 10. The plot of reflection coefficient magnitude of selected design 41 x 54 when the antenna is placed on human body phantoms, human arm, and in the free space.

In addition, Table 3 shows measured and simulated radiation efficiency, and simulated maximum 10 g average SAR for design 41 x 54 at 2.44 GHz. In the Fig.

11 are presented 3D radiation patterns of the selected design at 2.44 GHz in four different conditions.

Table 3: Radiation efficiency (%) and maximum 10 g average SAR (W/kg) of the optimized wearable antenna

Phantom	Semisolid	Liquid	Three-Layer	Free Space
Measured RE (%)	50.21	49.87	-	58.53
Simulated RE (%)	57.73	56.55	54.60	64.36
Simulated SAR (W/kg)	0.112	0.093	0.085	-

From Fig. 11 can be seen that the 3D radiation patterns are very similar even with three different body phantoms except for minor differences in the direction of the phantom (backward direction). The antenna in the free space has a 7.23 dB front-to-back ratio, which increases to 16.27 dB, 17.55 dB, and 23.38 dB when the antenna is placed on a three-layer semisolid, on a homogeneous semisolid, and on a liquid phantom, respectively. In the backward direction the lowest radiation is obtained for liquid phantom, due to the larger size and attenuation. The peak antenna gain is 5.565 dBi on the homogeneous semisolid, 4.570 dBi on three-layer, and 5.225 dBi on the liquid phantom, while in the free space the peak antenna gain is 4.504 dBi. The peak gain of the antenna increases (about 1 dB) when the antenna is placed on a phantom due to reflections of propagating waves from the phantom, however the efficiency is decreased [1].

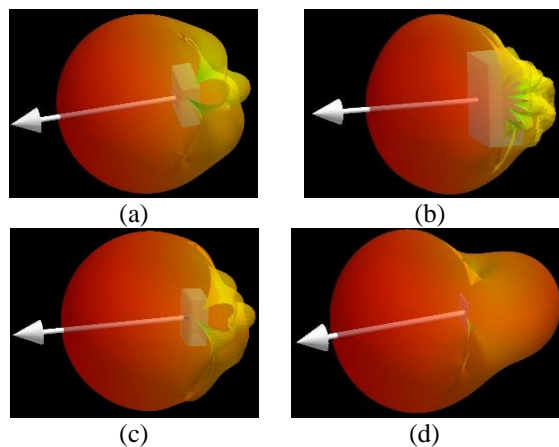


Fig. 11. 3D radiation pattern of selected design 41 x 54: (a) on the semisolid phantom, (b) on the liquid phantom, (c) on the three-layer phantom, and (d) in the free space.

V. CONCLUSION

In conclusion, we have proposed a novel algorithm to design-and-optimization of flexible wearable antennas

with high radiation efficiency and low SAR, that takes into account the dielectric loading of the human body. It provides a list of feasible antenna designs, not just a single solution and identifies the optimal wearable antenna design. The proposed algorithm has been validated using a planar dipole antenna with a reflector placed on a homogeneous semisolid phantom, a three-layer phantom and on a liquid phantom. The optimal antenna design was constructed, and antenna performance was studied under different conditions. The antenna shows robust on-body performances. Measured results demonstrate that a bandwidth of 118 MHz on semisolid phantom, 119 MHz on the liquid phantom, 119 MHz on the human arm, and 95 MHz in the free space is achieved. Moreover, measured radiation efficiency of 50.21%, 49.87%, and 58.53% is realized when the antenna is placed on the surface of semisolid and liquid phantom, and in the free space, respectively. Hence, optimization results achieved with described algorithm show that antenna size reduction is obtained without compromise in radiation efficiency, bandwidth and SAR. The presented algorithm can be quickly adopted in practice and applied to any wearable antenna structure.

The next step of the research work is to apply the algorithm in the case of more complex wearable antennas such a fractal antennas or antenna over a metasurface.

ACKNOWLEDGMENT

The authors would like to acknowledge the support of King Khalid University for this research through a Grant # RCAMS/KKU/006-18 under the Research Center for Advanced Materials Science at King Khalid University, Saudi Arabia and the University of Chemical Technology and Metallurgy, Sofia, Bulgaria.

REFERENCES

- [1] P. Hall and Y. Hao, *Antennas and Propagation for Body-Centric Wireless Communications*, 2nd ed., Artech House, London, 2012.
- [2] Q. H. Abbasi, M. U. Rehman, K. Qaraqe, and A. Alomainy, *Advances in Body-Centric Wireless Communication: Applications and State-of-the-Art*, IET, London, 2016.
- [3] N. F. M. Aun, P. J. Soh, A. A. Al-Hadi, M. F. Jamlos, G. A. E. Vandenbosch, and D. Schreurs, "Revolutionizing wearables for 5G," *IEEE Microwave Magazine*, vol. 18, no. 3, pp. 108-124, May 2017.
- [4] A. Y. I. Ashyap, Z. Z. Abidin, et al., "Inverted E-shaped wearable textile antenna for medical applications," *IEEE Access*, vol. 6, pp. 1-9, June 2018.
- [5] K. Ito, N. Haga, M. Takahashi, and K. Saito, "Evaluations of body-centric wireless communication channels in a range from 3 MHz to 3 GHz,"

- Proceedings of the IEEE*, vol. 100, no. 7, pp. 2356-2363, July 2012.
- [6] W. -C. Chen, B. DeLong, R. Vilku, and A. Kiourti, "Enabling batteryless wearables and implants," *ACES Journal*, vol. 33, no. 10, pp. 1106-1108, Oct. 2018.
- [7] S. Dumanli, L. Sayer, E. Mellios, X. Fafoutis, G. S. Hilton, and I. J. Craddock, "Off-body antenna wireless performance evaluation in a residential environment," *IEEE Trans. on Antennas and Propag.*, vol. 65, no. 11, pp. 6076-6084, Nov. 2017.
- [8] G. Conway, S. Cotton, and W. Scanlon, "An antennas and propagation approach to improving physical layer performance in wireless body area networks," *IEEE J. on Selected Area in Comm.*, vol. 27, no. 1, pp. 27-36, Jan. 2009.
- [9] A. Pellegrini, A. Brizzi, et al., "Antennas and propagation for body-centric wireless communications at millimeter-wave frequencies: A review," *IEEE Antennas and Propag. Magazine*, vol. 55, no. 4, pp. 262-287, Aug. 2013.
- [10] H. Khaleel, *Innovation in Wearable and Flexible Antennas*, WIT press, Southampton, 2015.
- [11] Ł. Januszkiewicz, P. D. Barba, and S. Hausman, "Optimization of wearable microwave antenna with simplified electromagnetic model of the human body," *OpenPhys.*, vol. 15, pp. 1055-1060, Nov. 2017.
- [12] A. Zare and S. Baghaie, "Application of ant colony optimization algorithm to pattern synthesis of uniform circular antenna array," *ACES Journal*, vol. 30, no. 8, pp. 810-818, Aug. 2015.
- [13] P. Rocca and R. Haupt, "Biologically inspired optimization of antenna arrays," *ACES Journal*, vol. 29, no. 12, pp. 1047-1059, Dec. 2014.
- [14] K. Fertas, H. Kimouche, M. Challal, H. Aksas, R. Aksas, and A. Azrar, "Design and optimization of a CPW-fed tri-band patch antenna using genetic algorithms," *ACES Journal*, vol. 30, no. 7, pp. 754-759, July 2015.
- [15] Z. Li, Y. Erdemli, J. Volakis, and P. Papalambros, "Design optimization of conformal antennas by integrating stochastic algorithms with the hybrid Finite-Element method," *IEEE Trans. on Antennas and Propag.*, vol. 50, no. 5, pp. 676-684, May 2012.
- [16] D. Prado, J. Álvarez, M. Arrebola, M. Pino, R. Ayestarán, and F. Las-Heras, "Efficient, accurate and scalable reflectarray phase-only synthesis based on the Levenberg-Marquardt algorithm," *ACES Journal*, vol. 30, no. 12, pp. 1246-1255, Dec. 2015.
- [17] X. Travassos, D. Vieira, and A. Lisboa, "Antenna optimization using multiobjective algorithm," *ISRN Communications and Networking*, vol. 2012, pp. 1-8, 2012.
- [18] P. Nepa and H. Rogier, "Wearable antennas for off-body radio links at VHF and UHF bands: Challenges, the state of the art, and future trends below 1 GHz," *IEEE Antennas and Propag. Magazine*, vol. 57, no. 5, pp. 30-52, Oct. 2015.
- [19] N. H. M. Rais, P. J. Soh, F. Malek, S. Ahmad, N. B. M. Hashim, and P. S. Hall, "A review of wearable antenna," *Loughborough Antennas & Propagation Conference*, pp. 225-228, Nov. 2009.
- [20] B. Gupta, S. Sankaralingam, and S. Dhar, "Development of wearable and implantable antennas in the last decade: A review," in *Proceedings of the 10th Mediterranean Microwave Symposium (MMS '10)*, pp. 251-267, Aug. 2010.
- [21] S. Dhupkariya, V. K. Singh, and A. Shukla, "A review of textile materials for wearable antenna," *J. Microwave Eng. Technol.*, vol. 1, no. 3, pp. 2349-9001, Oct. 2015.
- [22] C. A. Balanis editor, *Modern Antenna Handbook*, John Wiley & Sons, Inc., Hoboken, 2008.
- [23] A. Al-Sehemi, A. Al-Ghamdi, N. Dishovsky, N. Atanasov, and G. Atanasova, "On-body of a compact planar antenna on multilayer polymer composite for body-centric wireless communications," *AEU – International Journal of Electronics and Communications*, vol. 82, pp. 20-29, Dec. 2017.
- [24] T. Björninen, "Comparison of three body models of different complexities in modelling of equal-sized dipole and folded dipole wearable passive UHF RFID tags," *ACES Journal*, vol. 33, no. 6, pp. 706-709, June 2018.
- [25] EN 62209-2, *Human exposure to radio frequency fields from hand-held and body mounted devices – Human models, instrumentation, and procedures - Part 2: Procedure to determine the specific absorption rate (SAR) for wireless communication devices used in close proximity to the human body (frequency range of 30 MHz to 6 GHz)*, IEC, 2010.
- [26] *IEEE for Recommended Practice for Determining the Peak Spatial-Average Specific Absorption Rate (SAR) in the Human Head from Wireless Communications Devices: Measurement Techniques*, IEEE Standard 1528, 2003.
- [27] FCC, *SAR measurement requirements for 100 MHz to 6 GHz*, Aug. 2015.
- [28] L. Chen, C. Ong, C. Neo, V. V. Varadan, and V. K. Varadan, *Microwave Electronics: Measurement and Materials Characterization*, 1st ed., John Wiley & Sons, Ltd., 2004.
- [29] https://transition.fcc.gov/fcc-bin/dielec_file



Abdullah G. Al-Sehemi is a Professor in the Department of Chemistry King Khalid University, Saudi Arabia. He received his Ph.D. from University of Leicester, UK. He is currently Member of the Saudi Consultative Council. He was the Dean of Scientific Research and

Director of The Research Center for Advanced Materials Science (RCAMS). He is an author of over 200 publications, co-inventor of several patents and the editor of 6 books. He is working experimentally and computationally in the field of advanced functional materials, nanomaterials, stereochemistry, and drug design.



Ahmed A. Al-Ghamdi is a Staff Member at King Abdul Aziz University (KAU), Faculty of Science, Physics Department. He obtained his B.Sc. in Physics from KAU at 1981 and master's degree in 1985 from Tulane University, USA.

The Ph.D. degree was obtained in

1990 from Sussex University, UK, in point defects created by ion implantation. He has 26 years of experience in academic and research activities in solid state physics. He worked in the various field of solid physics applications including photodiodes, gas sensors, biosensors, and various another field of applications. He is currently working in synthesis, characterization and applications in composites and nanocomposites.



Nikolay T. Dishovsky received the Ph.D. degree from the University of Chemical Technology and Metallurgy, Sofia, in 1983 and the Doctor of Science Degree from the same university in 1997. Since 2000 he is a Full Professor and Head of the Department of Polymer

Engineering at the University of Chemical Technology and Metallurgy. He is the author of 8 books, more than 230 articles, and more than 45 patents for inventions. Dishovsky was a recipient of the Bulgarian Patent Office award for the Inventor of the Year 2015. His research interests include fillers and filled elastomers, rubber based nanocomposites, rubber based sensors and microwave absorbers.



Nikolay T. Atanasov received the M.Sc. and Ph.D. degrees from the Technical University of Sofia, Sofia, Bulgaria, in 1999 and 2013, respectively.

He is currently an Associate Professor in the Department of Communication and Computer Engineering, South-West University 'Neofit Rilski', Blagoevgrad, Bulgaria. His research interests include computational electrodynamics, SAR computation, design of antennas for wireless devices, medical diagnostic and therapeutic applications of EM. He is particularly interested in the characterization of the electromagnetic properties of the materials at microwave frequencies and investigation of the potential of conductive composites for the antenna applications.



Gabriela L. Atanasova received the M.Sc. and Ph.D. degrees from the Technical University of Sofia, Sofia, Bulgaria, in 1999 and 2013, respectively.

She is an Associate Professor in the Department of Communication and Computer Engineering, South-West University 'Neofit Rilski', Blagoevgrad, Bulgaria. Her research interests encompass theoretical and experimental studies for modeling interactions between EM fields and biological systems, as well as methods for the computer-aided analysis and design of high-frequency structures and antennas.